To further evaluate the direct pressure communication effect, the porous forebody with small strakes was configured by covering various regions of the porous surface with tape in order to create a local solid region on the porous forebody. The surface that has been taped over will be referred to as solid. The normal force and side force characteristics of several geometries are presented in Fig. 3.

Data are presented in Fig. 3 for the porous, solid upper right quadrant, solid right side, solid upper right quadrant with solid bottom, and the solid with the small strakes. The normal force data show that a solid top right quadrant contributes approximately one-half of the increment in normal force between the porous and solid forebodies with small strakes. The data show that a porous lower surface significantly influences the effectiveness of passive porosity to alleviate the asymmetric loading on the upper surface. The side force data show that upper surface passive porosity in combination with lower surface passive porosity provides improved effectiveness over upper surface passive porosity alone. This is especially evident for the configuration with a solid lower surface and solid top right quadrant.

Concluding Remarks

An experimental investigation to assess the effectiveness of passive porosity to change the pressure loading with free and fixed crossflow separation was conducted on a 5.0-caliber tangent-ogive forebody in the NASA Langley Research Center 14- by 22-ft Subsonic Wind Tunnel. The data show that the effectiveness of passive porosity to modify the forces for forced crossflow separation conditions is similar to that observed for the free crossflow separation condition. The data also show that the effectiveness of passive porosity to change the forces is significantly enhanced with the presence of large positive pressures on the porous surface. A preliminary look at the effect of plenum geometry showed that the effectiveness of the passive porosity system can be degraded if communication between high- and low-pressure regions is restricted.

References

[1]Nagamatsu, H. T., and Orozco, R. D., "Porosity Effect on Supercritical Airfoil Drag Reduction by Shock Wave Boundary Layer Control," AIAA Paper 84-1682, June 1984.

[2]Theide, P., Krogmann, P., and Syanewsky, E., "Active and Passive Shock/Boundary Layer Interaction Control on Supercritical Airfoils," AGARD-CP-365, 1984.

[3]Bahi, L., and Ross, J. M., "Passive Shock Wave/Boundary Layer Control for Transonic Airfoil Drag Reduction," AIAA Paper 83-0137, Jan. 1983.

[4]Chen, C.-L., Chow, C.-Y., Van Dalsem, W., and Holst, T., "Computation of Viscous Transonic Flow over Porous Airfoils," AIAA Paper 87-0359, July 1987.

[5]Olling, C. R., and Dulikravich, G. S., "Porous Airfoils Analysis Using Viscous-Inviscid Coupling at Transonic Speeds," *International Journal of Numerical Methods in Fluids*, Vol. 7, Feb. 1987, pp. 103–109.

[6]Wilcox, F. J., "Experimental Investigation of the Effects of a Porous Floor on Cavity Flow Fields at Supersonic Speeds," NASA TP 3032, March 1990.

[7]Hall, R. M., Erickson, G. E., Banks, D. W., and Fisher, D. F., NASA High Angle of Attack Technology Conf., Hampton, VA, Oct.–Nov. 1990.

[8]Allen, H. J., and Perkins, E. W., "A Study of the Effects of Viscosity on Flow over Slender Inclined Bodies of Revolution," NACA TR 1048, 1951.

[9]Letko, W., "A Low-Speed Experimental Study of the Directional Characteristics of a Sharp Nosed Fuselage Through a Large Angle of Attack Range at Zero Angle of Sideslip," NACA TN 2911, 1953.

[10]Coe, P. L., Jr., Chambers, J. R., and Letko, W., "Asymmetric Lateral-Directional Characteristics of Pointed Bodies of Revolution at High Angles of Attack," NASA TN D-7095, 1973.

[11]Jorgensen, L. H., and Nelson, E. R., "Experimental Aerodynamic Characteristics for a Cylindrical Body of Revolution with Various Noses at Angles of Attack from 0° to 58° and Mach Numbers from 0.6 to 2.0," NASA TM X-3128, 1974.

[12]Jorgensen, L. H., and Nelson, E. R., "Experimental Aerodynamic Characteristics for a Cylindrical Body of Revolution with Side Strakes and Various Noses at Angles of Attack from 0° to 58° and Mach Numbers from 0.6 to 2.0," NASA TM X-3130, March 1975.

[13]Bauer, S. X. S., and Hemsch, M. J., "Alleviation of Side Force on Tangent Ogive Forebodies Using Passive Porosity," AIAA Paper 92-2711, June 1992.

[14]Gentry, G. L., Jr., Quinto, P. F., Gatlin, G. M., and Applin, Z. T., "The Langley 14- by 22-Foot Subsonic Tunnel: Description, Flow Characteristics, and Guide for Users," NASA TP-3008, Sept. 1990.

Vortical Flow Structure near the F/A-18 LEX at High Incidence

B. H. K. Lee* and N. R. Valerio†
Institute for Aerospace Research, Ottawa, Ontario K1A 0R6, Canada

Introduction

THE high degree of maneuverability of the F/A-18 at subsonic flight speeds is largely credited to the leading-edge extension (LEX) that generates large nonlinear lift at high angles of attack. The lift enhancement arises from vortex generated by the rolling-up of separated flow at the highly swept leading edge of the LEX. Ultimately, the two LEX vortices burst and the resulting turbulent flow impacts on the tail section of the aircraft causing severe structural damage.[1] Some alleviation of the loads on the aircraft horizontal stabilizers and vertical fins can be achieved by the installation of a streamwise fence on the LEX.[2] The role of the fence is to alter the flow structure of the LEX vortices.

Flow visualization studies[3,4] of the flow in the vicinity of the F/A-18 LEX show a pair of corotating vortices emerging downstream of the fence. However, a mechanism explaining the presence of these vortices is not elucidated in Refs. 3 and 4 due to limitations in the experimental techniques used.

This Note attempts to provide further insight into the complex flow structure generated by the LEX and fence through a study of the topology of the surface skin friction lines. The experiment was carried out on a 6% scale rigid model of the F/A-18 in the IAR 1.5-m Trisonic Blowdown Wind Tunnel. Various angles of attack were investigated. The results presented herein are for $M = 0.6$ and $\alpha = 30$ deg.

Model and Experimental Technique

The model is described in detail in Ref. 2. The leading- and trailing-edge flap deflections were set at 34 and 0 deg, respectively. The horizontal stabilizer angle was positioned at −9 deg for the wind-tunnel investigation. Models of the Aim 9 missiles were mounted at the wingtips.

For flow visualization studies, oil dots, formed by mixing SAE 30-grade motor oil with carbon black, were deposited on the upper surface of the LEX and on both surfaces of the

Received Nov. 2, 1993; revision received Nov. 29, 1993; accepted for publication Dec. 3, 1993.

*Senior Research Officer, National Research Council, High Speed Aerodynamics Laboratory; also, adjunct Professor, Department of Mechanical Engineering, University of Ottawa, Ottawa, Ontario K1N 6N5, Canada. Associate Fellow AIAA.

†Guest Worker, National Research Council, Department of Mechanical Engineering, McGill University, Montreal, Quebec H3A 2K6, Canada.

fence. The trajectories traced by the oil are called streaks or skin friction lines, and they indicate the behavior of the flow on the surface. An excellent description of the oil dot technique in the study of three-dimensional vortical flow topology is given by Peake and Tobak.[5]

To achieve good visualization results, the oil dots were spaced sufficiently far apart so that the oil flow at the start of a wind-tunnel run would not interfere with the streaks when steady flow was established. This resulted in some loss of resolution in regions of rapid spatial changes in flow structure. The oil dot size used in this investigation was approximately 0.02 in. diam. Best results were achieved for a wind-tunnel run of approximately 30-s duration at $M = 0.6$ and a dynamic pressure of 4 psi. To obtain a permanent record of the flow visualization, white paper with an adhesive backing, such as that used for labels, was put on the wing surface after a wind-tunnel run. Care was exercised so that no air pockets were formed between the paper and the model surface. In removing the paper, uniform tension was applied so that the paper would not be overstretched. By using label papers with different adhesive backings, a suitable one was found to give the best results for this particular model surface finish. This technique could transcribe the very fine details of the oil dot streak lines onto the paper, and was found to be much better than the usual procedure of photographing the streak lines on films.

Results and Discussion

Figure 1 shows the skin friction lines in the vicinity of the fence on the starboard LEX at $M = 0.6$ and $\alpha = 30$ deg. The lines due to the starting flow were not included in this figure. The locations of the attachment line A_1 and the separation line S_1 can be determined from the diverging and converging patterns of the skin friction lines, respectively. These two lines (A_1 and S_1) are associated with the primary rolled-up LEX vortex and the induced secondary vortex. The oil dot technique does not give sufficient resolution to detect any surface features attributable to the tertiary vortex reported in the literature.[6] The low resolution also does not allow for the line S_1 to remain identifiable near the fence.

In the vicinity of the fence, on the inboard side, the location of a second separation line S_2 is observed originating from the saddle point S_p. The focus N_1 can be deduced from the local direction of the skin friction lines on the LEX.

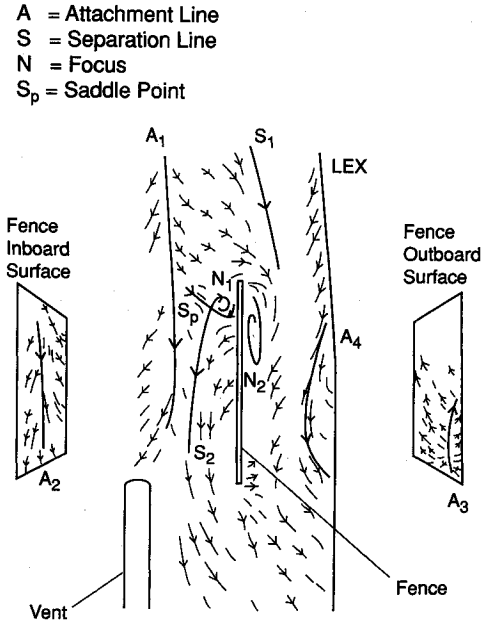

Fig. 1 LEX surface flow visualization at $M = 0.6$ and $\alpha = 30$ deg.

The focus and saddle point indicate a vortex that detaches from the surface. This vortex then progresses along the fence in the downstream direction, as evidenced by S_2 on the LEX and the attachment line A_2 found on the inboard surface of the fence. The vortex is due to the effect of the pressure gradient induced by the fence on the strong circumferential flow of the primary LEX vortex.

On the outboard side of the fence, the presence of focus N_2 is indicated by the direction of the skin friction lines and the accumulation of a small amount of oil near the junction of the fence and the LEX. The attachment line A_3 on the fence's surface is determined from the diverging skin friction lines. The vortex causing this line is fed by vorticity being generated at the upstream vertical and horizontal edges of the fence. It rotates in a direction contrary to that of the primary LEX vortex. This fence-generated vortex is also observed from numerical computations using a Navier-Stokes code.[7]

Near the LEX leading edge, the diverging skin friction lines show the location of the attachment line A_4. This indicates a vortex fed by the shear layer originating from the LEX leading edge, turning in the same direction as the primary vortex, as observed by Thompson[3] and Erickson et al.[4] A separation line is deduced to exist between the lines A_3 and A_4.

The surface skin friction lines in Fig. 1 and the results from Refs. 3 and 4 indicate that the off-surface vortical flow structure at a position near the end of the fence is as sketched in Fig. 2. The position of A_1 is fixed by the primary LEX vortex V_1. At the junction of the fence and the LEX, on the inboard side, a vortex V_2 is formed due to the effect of the pressure gradient generated by the fence on the circumferential flow of the primary LEX vortex. S_2 and A_2 associated with this vortex are denoted in the figure. A vortex V_3 rolls up from the top edge of the fence. The position of the A_3, which results from this vortex, is shown on the outboard surface of the fence. These lines are also depicted in Fig. 1. Since a separation line is deduced to exist between the lines A_3 and A_4 from an analysis of the surface flow structure in Fig. 1, the vortex V_5 is included to satisfy topological rules.[5]

A_4 is associated with a second corotating vortex V_4. A possible mechanism in the formation of this vortex is as follows. Near the beginning of the fence, the vortex V_3, which in-

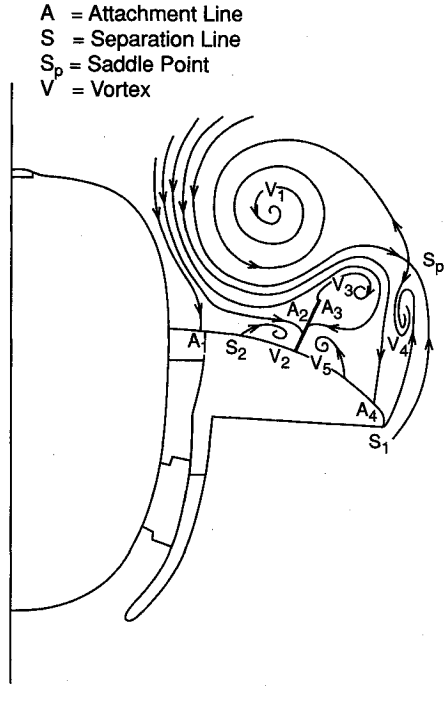

Fig. 2 LEX off-surface flow topology near the end of the fence at $M = 0.6$ and $\alpha = 30$ deg.

creases in strength downstream, approaches the shear layer generated at the LEX leading edge. The interaction causes a "kink," as observed by Thompson,[3] to develop in the shear layer. The kink, with the shear layer feeding into it, later develops into V_4 further downstream. As a result, an off-surface saddle point S_p exists, and the shear layer generated at the LEX leading edge no longer feeds vorticity into the primary V_1. A similar surface flow structure is observed from wind-tunnel tests carried out at $M = 0.6$ and 25 deg $\leq \alpha \leq$ 35 deg.

Acknowledgments

The authors wish to acknowledge the support from the Institute for Aerospace Research and the Natural Sciences and Engineering Research Council of Canada.

References

[1]Lee, B. H. K., Brown, D., Zgela, M., and Poirel, D., "Wind Tunnel Investigation and Flight Tests of Tail Buffet on the CF-18 Aircraft," Specialists' Meeting on Aircraft Dynamic Loads Due to Flow Separation, AGARD CP-483, Sorrento, Italy, April 1990, pp. 1.1–1.26.

[2]Lee, B., and Brown, D., "Wind Tunnel Studies of F/A-18 Tail Buffet," *Journal of Aircraft*, Vol. 29, No. 1, 1992, pp. 146–152.

[3]Thompson, D. H., "Water Tunnel Flow Visualization of Vortex Breakdown over the F/A18," Aeronautical Research Lab., Flights Mechanics Rept. 179, Australia, Dec. 1990.

[4]Erickson, G. E., Hall, R. M., Banks, D. W., Del Frate, J. H., Schriener, J. A., Hanley, R. J., and Pulley, C. T., "Experimental Investigation of the F/A-18 Vortex Flows at Subsonic Through Transonic Speeds, Invited Paper," AIAA Paper 89-2222, July/Aug. 1989.

[5]Peake, D. J., and Tobak, M., "Three-Dimensional Interactions and Vortical Flows with Emphasis on High Speeds," NASA TM 81169, March 1980.

[6]Fischer, D. F., Del Frate, J. H., and Richwine, D. M., "In-Flight Flow Visualization Characteristics of the NASA F-18 High Alpha Research Vehicle at High Angles of Attack," NASA TM 4193, May 1990.

[7]Rizk, Y. M., Guruswamy, G., and Gee, K., "Numerical Investigation of Tail Buffet on F-18 Aircraft," AIAA Paper 92-2673, June 1992.

Minimum Sink-Speed in Power-Off Glide

Edmund V. Laitone*
University of California, Berkeley, Berkeley, California 94720

Nomenclature

A = wing aspect ratio, $(\text{span})^2/S = b^2/S$
C_D = airplane drag coefficient, $D/(\frac{1}{2}\rho V^2 S)$
C_L = airplane lift coefficient, $L/(\frac{1}{2}\rho V^2 S)$
D = drag force parallel to flight path
e = Oswald const. for best fit to drag polar data, Eq. (1)
$\mathring{h}$ = sink-speed, dh/dt
L = lift force perpendicular to flight path
S = wing planform area
V = velocity along flight path
W = airplane weight
δ = $C_{D_e}/(\pi Ae)$
θ = glide angle below horizontal
ρ = atmospheric mass density

Subscripts
mp = minimum power required for steady level flight
* = flight conditions for maximum, lift/drag

Received Feb. 17, 1993; revision received Oct. 24, 1993; accepted for publication Nov. 20, 1993.

*Emeritus Professor, Department of Mechanical Engineering. Fellow AIAA.

Introduction

SOME aeronautical engineers who have participated in glider competition have insisted that the minimum sink-speed $\mathring{h}$ occurs at a trim velocity that is less than V_{mp}, which is the velocity corresponding to minimum power required for steady level flight. It is usually assumed that the trim lift coefficient $C_{L,\text{mp}}$ gives the minimum sink-speed for any airplane in power-off glide. Without extensive wind-tunnel or flight data, V_{mp} can be estimated as $V_*/3^{1/4}$, where V_* is the trim velocity that produces the minimum glide angle θ_* in a steady glide with zero thrust. The following analysis uses the theoretical drag polar to derive a new relation that proves that the minimum sink-speed does occur with a trim lift coefficient that is slightly greater than $C_{L,\text{mp}}$.

Analysis

The well-known airplane drag polar may be written as

$$C_D = C_{D_e} + C_L^2/\pi Ae \tag{1}$$

where the zero lift drag coefficient C_{D_e}, and the airplanes effective aspect ratio $Ae = eb^2/S$, should be selected so as to provide the best straight line approximation for wind-tunnel or flight data when plotted on a graph of C_D vs C_L^2. As shown by Laitone,[1] C_{D_e} is usually slightly less than minimum drag coefficient found in wind-tunnel tests, and the Oswald effective aspect ratio factor is usually $1 > e > 0.9$ for properly designed aircraft, in the normal flight range, well above the stalling speed.

The maximum lift-drag ratio from Eq. (1) is given by the lift coefficient C_{L_*} obtained from

$$\frac{d}{dC_L}\left(\frac{C_D}{C_L}\right) = -\frac{C_{D_e}}{C_{L_*}^2} + \frac{1}{\pi Ae} = 0$$
$$C_{L_*} = (\pi Ae C_{D_e})^{1/2} \quad \text{and} \quad C_{D_*} = 2C_{D_e} \tag{2}$$

In a steady-state glide with zero thrust, the glide angle θ is given by Fig. 1 as

$$\theta = \tan^{-1}(C_D/C_L) = \sin^{-1}(\mathring{h}/V_\infty) = \cos^{-1}(L/W)$$
$$V_\infty = (W\cos\theta/\tfrac{1}{2}\rho S C_L)^{1/2} \quad \text{and} \quad \mathring{h} = DV_\infty/W \tag{3}$$

The trim lift coefficient C_L is constant during the steady-state glide at flight path velocity V_∞.

Obviously the minimum glide angle is given by the maximum lift-drag ratio at $C_L = C_{L_*}$ as

$$\theta_* = \tan^{-1}(C_{D_*}/C_{L_*}) = \tan^{-1}2(C_{D_e}/\pi Ae)^{1/2} \tag{4}$$

However, the minimum sink-speed is related to the minimum power mp $= D_{\text{mp}}V_{\text{mp}}$, rather than the maximum lift-drag ratio that gave the minimum glide angle. The equivalent to the power in a steady-state glide at the constant velocity V_∞ varies with the glide angle as

$$DV_\infty = \tfrac{1}{2}\rho S C_D V_\infty^3 = W^{3/2}(\tfrac{1}{2}\rho S)^{-1/2} C_D C_L^{-3/2}(\cos\theta)^{3/2} \tag{5}$$